Mindlin (2/3)

NSC92-2211-E-009-043-

92 08 01 93 07 31

'

93 5 26

Mindlin (2/3)
Investigation in Vibrations of Mindlin Plates with Stress
Singularities(2/3)

( )

93 5 17

（　　　　　　　　　　　　　　　　　　. . ）　　　　　　Mindlin

Mindlin

（eigenfunction expansion）

Mindlin

92　8　　93　7　　　　　　　　　　　　　　　　Ritz

（cantilevered skewed plates）（

）

Ritz

93　8　　94　7

Mindlin　　　　　　　　　　　　　　Ritz

1. Abstract

Plates are widely used components in engineering applications for civil engineering, mechanical engineering, and aerospace engineering. The Mindlin plate theory is often applied to describe the behaviors of plates. It is well known that stress singularities arise in the mathematical solutions of plate problems, which can be due to concentrated forces and moments, discontinuities in edge conditions or sharp corner. It has been pointed out and numerically shown that if singularities due to discontinuities in edge conditions or sharp corners are not properly considered in numerical solutions, significant errors will occur in the calculated global behavior of plates, such as static deflection, free vibration frequencies, forced dynamic response, and critical buckling load. However, there is no comprehensive study in the stress singularities for the Mindlin plate theory. Consequently, it is also short of accurate numerical solutions for the plates with stress singularities. It is the main purpose of the three-year proposal to investigate the stress singularity behaviors of Mindlin plates due to discontinuities in edge conditions or sharp corner and apply these results to some well known numerical solution techniques to solve some complicate vibration problems involving stress singularities.

In the first year, eigenfunction expansion approach was applied to find the asymptotic solution for stress singularity behavior in the Mindlin plate theory. The singularity orders corresponding to various combinations of edge conditions were determined and expressed in graphic form. The results will be compared with those for thin plate theory.

In the second year, the obtained asymptotic solutions were used in the Ritz method and to solve the vibration problems such as sectorial plates and cantilevered skewed plates (including skewed triangular, parallelogram, and trapezoidal plates). We carried out the investigation on the effects of some geometric parameters, such as vertex angles and skewed angle et al., on the vibrations of such plates. Furthermore, the effects of the asymptotic solutions on the Ritz approach were also investigated.

In the third year, the obtained asymptotic solutions will be further used in conventional finite element approach. A new way to incorporate the asymptotic solutions into the finite

element approach will be proposed, so that the proposed approach can be broadly applied to solve a variety of vibration problems with complicated geometry and stress singularities. The analyses will also be performed on the vibrations of sectorial plates and cantilevered skewed or rectangular plates with a rectangular cutout or crack.

Keywords: Mindlin plate theory, stress singularities, eigenfunction expansion, Ritz Method, Finite Element Approach, Thick Plate, Vibration Analysis

2. Motive and Goal

In the second year of this project, the asymptotic solutions obtained in the first year of this project were used in the Ritz method and to solve the vibration problems such as sectorial plates and cantilevered skewed plates (including skewed triangular, parallelogram, and trapezoidal plates). Since this report is for mid-term report, the work on analyzing the vibrations of cantilevered skewed plates will be emphasized, while the work on sectorial plates will be included in the final report.

A cantilevered skewed trapezoidal plate, as depicted in Fig.1, has been found in numerous engineering applications, including aircraft and guided missiles. A cantilevered skewed triangular plate or parallelogram plate can be treated as a special case of a trapezoidal plate. In Fig.1, c/b=0 represents a skewed triangular plate while c/b=1 specifies a parallelogram plate. Because of the complexity of the geometrical shape and the boundary conditions, no exact solution is tractable for the free vibrations of such plates. Many numerical solutions, based on classical thin plate theories, have been published for such plates. Leissa [1-4] reviewed much of the earlier work in this field, while more recent work was mentioned in references 5 and 6.

Shear deformation and rotary inertia are well known to be important to any analysis of moderately thick plates or in determining the higher vibration frequencies of thin plates. Nevertheless, rather few results have been published on the vibration frequencies of skewed triangular, trapezoidal and parallelogram plates as derived using plate theories including the effects of shear deformation and rotary inertia. McGee and Butalia [7] presented a higher-order finite element plate formulation for analyzing the vibrations of skewed trapezoidal and triangular thick plates. Karunasena *et al*. [8] applied the pb-2 Rayleigh-Ritz method to elucidate the vibrations of cantilevered skewed triangular Mindlin plates.

To investigate vibrations of parallelogram plates, Kanaka Raju and Hinton [9] and Liew et al. [10] employed Mindlin plate theory, and used a finite element approach and pb-2 Rayleigh-Ritz method, respectively, while McGee and Leissa [11] used the Ritz method and three-dimensional elasticity theory. McGee and Butalia [12] thoroughly studied the vibrations of skew plates using nine-node Lagrangian isoparametric quadrilateral plate elements, based on three shear deformable thick plate theories.

Recently, Huang [13 and 14] showed that corner stress singularities arise in Mindlin plate theory and Reddy's refined plate theory when the vertex angle of a wedge with clamped and free boundary conditions along its radial edges exceeds approximately 60°. As shown in [5, 6] for cantilevered skewed thin plates, corner stress singularity behaviors have to be considered in numerical approaches in order to obtain accurate vibration frequencies. Nevertheless, in the aforementioned publications on cantilevered skewed triangular, trapezoidal and parallelogram Mindlin plates, numerical approaches have not numerical approaches stress singularities. In [12], finite element convergence studies of cantilevered skewed thick plates reveal that the accuracy of the results obtained using a specified mesh size declines as the skew angle is increased. Furthermore, Karunasena *et al*. [8] admitted that their results, obtained by the pb-2 Rayleigh-Ritz method, are not accurate for cantilevered skewed triangular Mindlin plates with large skew angles because their approach did not incorporate the effects of stress singularities. Accordingly, the vibrations of cantilevered trapezoidal plates must be reexamined, considering corner stress singularities.

The aim of this work is to present an accurate numerical solution for the free vibrations of

skewed cantilevered triangular, trapezoidal and parallelogram Mindlin plates using the Ritz method and considering the corner stress singularities. The Ritz method has been popularly applied to investigate the vibrations of structural components. For simplicity, polynomial functions are commonly selected as the admissible functions in the Ritz method. However, the Ritz method, involving a large number of polynomial functions, is well known to yield easily a generalized eigenvalue problem with an ill-conditioned matrix. In this work, "corner functions" are introduced into the admissible functions, which also include polynomial functions, to accelerate the convergence of solutions. The corner functions are established from the asymptotic solutions provided by Huang [13] for both moment and shear force singularities at a corner of a thick plate. Hence, the corner functions not only appropriately describe the singular behaviors at the clamped re-entrant corner of a skewed cantilevered plate, but also meet the clamped boundary conditions and free moment conditions around the re-entrant corner. Convergence studies are herein conducted for various skew angles to demonstrate the effects of corner functions on the accuracy of the numerical results. Accurate vibration frequencies of skewed cantilevered trapezoidal plates with various skew angles, aspect ratios (*a/b*), chord ratios (*c/b*) and thickness ratios (*h/b*) are reported and compared to the published results obtained by other researchers to improve the currently available data base.

3. Contents of the Research

3.1 Methodology

For the free vibration of a plate in Cartesian coordinates (*x, y*), the maximum strain energy (*V*max) and the maximum kinetic energy (*T*max) are (cf. [8]),

$$V_{\max} = \iint_A \frac{D}{2} \{ [\psi_{x,x}^2 + \psi_{y,y}^2 + 2\upsilon \psi_{x,x}\psi_{y,y} + \frac{1-\upsilon}{2}(\psi_{x,y} + \psi_{y,x})^2]$$

$$+ \frac{\kappa^2 Gh}{2}[(\psi_x + w_{,x})^2 + (\psi_y + w_{,y})^2]\} dA \tag{1}$$

$$T_{\max} = \frac{\omega^2}{2} \iint_A \{\rho h w^2 + \frac{\rho h^3}{12}(\psi_x^2 + \psi_y^2)\} dA \tag{2}$$

where w is the transverse displacement of the mid-plane; ψ_x and ψ_y are the bending rotations of the mid-plane normal in the x and y directions, respectively; h is the thickness of the plate; $D = Eh^3 /12(1-\upsilon^2)$ is the flexural rigidity; E is the modulus of elasticity; υ is Poisson's ratio ; κ^2 is the shear correction factor; G is the shear modulus, and ω is the vibration frequency.

The use of skew coordinates (ξ, η) (Fig.1) and oblique rotations, ψ_ξ and ψ_η is normally convenient in analyzing skew plates. They are related to orthogonal coordinates, x and y, and orthogonal rotations, ψ_x and ψ_y, by

$$\xi = x/\cos\beta , \quad \eta = y - x\tan\beta , \tag{3}$$

and

$$\psi_\xi = \psi_x + \psi_y \tan\beta , \quad \psi_\eta = \psi_y /\cos\beta , \tag{4}$$

where is the skew angle (Fig. 1). Equations (1-4) can be used to redefine *V*max and *T*max in the skew coordinates as

$$V_{\max} = \iint_A \{ \frac{D}{2} \{ \sec^2 \beta (\psi_{\xi,\xi} - \sin\beta \, \psi_{\xi,\eta} - \sin\beta \, \psi_{\eta,\xi} + \psi_{\eta,\eta})^2 -$$

$$2(1-\upsilon)[\psi_{\eta,\eta}\psi_{\xi,\xi} - \frac{1}{4}(\psi_{\xi,\eta} + \psi_{\eta,\xi})^2]\} +$$

$$\frac{\kappa^2 Gh}{2}[(\psi_\xi - \sin\beta\,\psi_\eta + \sec\beta\,w,_\xi - \tan\beta\,w,_\eta)^2 + (\cos\beta\,\psi_\eta + w,_\eta)^2\}dA \quad (5)$$

$$T_{\max} = \frac{\omega^2}{2}\iint_A \{\rho h w^2 + \frac{\rho h^3}{12}[(\psi_\xi - \sin\beta\,\psi_\eta)^2 + (\cos\beta\,\psi_\eta)^2]\}dA \quad (6)$$

where $dA = \cos\beta\,d\xi\,d\eta$.

In the Ritz method, the energy functional is defined as

$$\Pi = V_{\max} - T_{\max}. \quad (7)$$

$w(\xi,\eta)$, $\psi_\xi(\xi,\eta)$ and $\psi_\eta(\xi,\eta)$ in eqs. (6 and 7) are approximated by finite series of admissible functions, which satisfy the geometric boundary conditions under consideration, and expressed as

$$\psi_\xi(\xi,\eta) = \Psi_{\xi\,p}(\xi,\eta) + \Psi_{\xi\,c}(\xi,\eta), \quad (8a)$$

$$\psi_\eta(\xi,\eta) = \Psi_{\eta\,p}(\xi,\eta) + \Psi_{\eta\,c}(\xi,\eta), \quad (8b)$$

$$w(\xi,\eta) = W_p(\xi,\eta) + W_c(\xi,\eta), \quad (8c)$$

where $\Psi_{\xi\,p}$, $\Psi_{\eta\,p}$ and W_p consist of algebraic polynomials, and $\Psi_{\xi\,c}$, $\Psi_{\eta\,c}$ and W_c consist of corner functions, which account for the singular behaviors of moments and shear forces at re-entrant corner $\angle ABC$ in Fig.1. The polynomials in terms of skew co-ordinates are used; hence,

$$\Psi_{\xi\,p} = \sum_{i=1}^{I}\sum_{j=1}^{J} A_{ij}\xi^i\eta^{j-1}, \quad \Psi_{\eta\,p} = \sum_{i=1}^{I}\sum_{j=1}^{J} B_{ij}\xi^i\eta^{j-1}, \quad W_p = \sum_{i=1}^{I}\sum_{j=1}^{J} C_{ij}\xi^i\eta^{j-1}, \quad (9)$$

where A_{ij}, B_{ij} and C_{ij} are coefficients to be determined by minimizing Π.

Although the polynomials given in eq.(9) constitute a mathematically complete set of admissible functions and theoretically yield accurate values of the frequencies when I and J are large enough, numerical difficulties are very likely to occur when I and J are large. It is desirable to supplement the polynomial admissible functions with the corner functions, which properly represent the singularities, to accelerate the convergence of the solution.

The sets of corner functions are

$$\Psi_{\xi\,c}(\xi,\eta) = \sum_{k=1}^{K}\overline{A}_k\overline{\Psi}_{\xi\,k}(\xi,\eta), \quad \Psi_{\eta\,c}(\xi,\eta) = \sum_{k=1}^{K}\overline{B}_k\overline{\Psi}_{\eta\,k}(\xi,\eta), \quad W_c(\xi,\eta) = \sum_{n=1}^{N}\overline{C}_n\overline{W}_n(\xi,\eta) \quad ,$$
$$(10)$$

where $\overline{A}_k$, $\overline{B}_k$ and $\overline{C}_n$ are arbitrary coefficients, and $\overline{\Psi}_{\xi\,k}$, $\overline{\Psi}_{\eta\,k}$ and $\overline{W}_n$ are established from the asymptotic solutions presented in [13]. The asymptotic solutions [13] are expressed in terms of polar co-ordinates (r,θ) as shown in Fig.1, the displacement components in polar co-ordinates have to transform into those in skew co-ordinates, yielding,

$$\overline{\Psi}_{\xi\,k} = (\cos\theta + \tan\beta\sin\theta)\overline{\Psi}_{\theta\,k} + (\sin\theta - \tan\beta\cos\theta)\overline{\Psi}_{r\,k}, \quad (11a)$$

$$\overline{\Psi}_{\eta\,k} = (\sin\theta\,\overline{\Psi}_{\theta\,k} - \cos\theta\,\overline{\Psi}_{r\,k})/\cos\beta, \quad (11b)$$

$$\overline{W}_n = r^{\overline{\lambda}_n}\sin\overline{\lambda}_n\theta, \quad (11c)$$

where

$$\overline{\Psi}_{r\,k} = r^{\lambda_k}\{\cos(\lambda_k+1)\theta - k_1\eta_1\sin(\lambda_k+1)\theta - \cos(\lambda_k-1)\theta + \eta_1\sin(\lambda_k-1)\theta\}, \quad (12a)$$

$$\overline{\Psi}_{\theta\,k} = r^{\lambda_k}\{-\sin(\lambda_k+1)\theta - k_1\eta_1\cos(\lambda_k+1)\theta + k_1\sin(\lambda_k-1)\theta + k_1\eta_1\cos(\lambda_k-1)\theta\}, \quad (12b)$$

$$\eta_1 = -\frac{\lambda_k(1-\upsilon)\cos(\lambda_k+1)\alpha - (k_1(\lambda_k-1) - \lambda_k\upsilon - 1)\cos(\lambda_k-1)\alpha}{(k_1(\lambda_k-1) - \lambda_k\upsilon - 1)\sin(\lambda_k-1)\alpha - k_1\lambda_k(1-\upsilon)\sin(\lambda_k+1)\alpha}, \quad (12c)$$

$$k_1 = -\frac{2(1-\upsilon) + (1+\upsilon)(\lambda_k +1)}{2(1-\upsilon) - (1+\upsilon)(\lambda_k -1)}, \tag{12d}$$

$$r = \{(\frac{b}{2} - \eta)^2 + \xi^2 - 2\xi(\frac{b}{2} - \eta)\sin\beta\}^{1/2}, \tag{12e}$$

$$\theta = Tan^{-1}(\frac{\xi\cos\beta}{(b/2 - \eta) - \xi\sin\beta}), \tag{12f}$$

and   is the re-entrant angle (Fig. 1). The characteristic values λ_k and $\overline{\lambda}_n$ are, respectively, the roots of the following equations:

$$\sin^2\lambda_k\alpha = \frac{4 - \lambda_n^2(1+\upsilon)^2\sin^2\alpha}{(3-\upsilon)(1+\upsilon)}, \tag{13a}$$

and

$$\cos\overline{\lambda}_n\alpha = 0. \tag{13b}$$

Using the Ritz method, the free vibration problem is solved by substituting eqs. (9) and (11) into eqs.(5) and (6) and minimizing Π in eq.(7). Minimizing Π with respect to the undetermined coefficients A_{ij}, B_{ij}, C_{ij}, $\overline{A}_k$, $\overline{B}_k$, and $\overline{C}_n$ yields $3IJ+2K+N$ homogeneous, linear algebraic equations in terms of the undetermined coefficients, which results in the matrix form of a generalized eigenvalue problem. The eigenvalues correspond to the natural vibration frequencies.

3.2 Results and discussion

The frequencies obtained by the Ritz method should monotonically converge to the exact frequencies as upper bounds when a sufficient number of admissible functions are used, if the admissible functions are taken from a complete set of functions. This section addresses convergence studies which were carried out for cantilevered skewed triangular plates. All numerical results are presented in terms of the nondimensional frequency parameter Ω defined as $\omega a^2\sqrt{\rho h / D}$. The results are for materials with a Poisson ratio (υ) of 0.3.

Tables 1-2 present a convergence study of the non-dimensional frequency parameters of five skewed triangular plates (a/b=1; h/b=0.001 or 0.2; $\beta = 60^o$ or 75°). The shear correction factors were set equal to 5/6 to allow the present results to be compared with published data. The frequencies were obtained by increasing the number of polynomial terms in eq. (9) (e.g. (I,J)=(4,4), (5,5), …,(9,9)) and the number of corner functions in eq. (10) (e.g. $K=N$=0, 5, 10, and 15 for $\beta \geq 60^o$).

Tables 1-2 show that the frequencies monotonically converge to the exact ones from above as the number of polynomial terms or the number of corner functions increases. The results obtained using only polynomial terms ($K=N$=0) do not converge well for large skew angles ($\beta = 60^o$ or 75°). The convergence of the frequencies is significantly enhanced by augmenting the polynomial sets with an increasing number of corner functions, especially for a large skew angle. The improvement in the convergence of frequencies obtained by adding corner functions does not considerably change for different values of h/b. The results obtained using $I=J$=8 and $K=N$=10 are exact to at least three significant figures.

Some of the published results obtained by others are also given in Tables 1-2. Based on classical thin plate theory, McGee et al. [6] applied the Ritz method and added thin plate theory corner functions to the algebraic polynomial admissible displacement functions. Based on Mindlin plate theory, Karunasena et al. [8] obtained the natural frequencies of skewed triangular plates by using the Ritz method and 120 admissible polynomial functions for each of w, ψ_ξ and ψ_η. Comparing the presented results with those of McGee et al. [6] reveals that the present

converged results demonstrate the theoretical fact that the frequencies determined from Mindlin plate theory are less than those obtained from thin plate theory. However, the results of Karunasena *et al*. [8] violate this, indicating these results not accurate enough. Indeed, their frequencies are seen to be much too high for large skew angles ($\beta = 60^{o}$ and 75°). Karunasena *et al*. [8] acknowledged that the accuracy of their results become worse as the skewed angle increases because stress singularity effects at the re-entrant corner were not considered. Notably, the present solution does not show the shear locking phenomenon that is often found in a finite element approach when the Mindlin plate theory is applied to a thin plate.

The results of McGee and Butalia [7] in Table 3 were obtained using higher-order shear deformable plate theory and the finite element approach. No shear correction factor is involved. These results were obtained using 64 Lagrangian isoparametric plate elements with a total of 2448 degrees of freedom, whereas the present method used, at most, 222 degrees of freedom. The convergence studies in [7] indicate that these results may converge to only two significant figures. Generally reasonably good agreement is observed between the present results and those of McGee and Butalia [7], except in the cases of plates with $\beta = 75^{o}$. Notably, McGee and Butalia [7] conceded that the stress singularity at the re-entrant corner should be incorporated into their finite element modeling of highly skewed plates, when they found that their results for thin plates exceeded those obtained by applying thin plate theory [6] using the Ritz method.

Figure 2 shows the nodal patterns for parallelogram plates with $\beta = 45^{o}$ and 75° and *h/b*=0.1. The nodal patterns for $\beta = 75^{o}$ are first shown in the literature. One can find that the nodal patterns strongly depend on the skew angle, especially for higher modes.

4. Concluding Remarks

This work has demonstrated a novel Ritz procedure to determine accurately the natural frequencies of skewed cantilevered triangular, trapezoidal and parallelogram plates based on Mindlin plate theory. The proposed procedure incorporates a mathematically complete set of admissible polynomials in conjunction with admissible corner functions that not only properly describe the singular behaviors of moments and shear forces at the re-entrant clamped corner, but also satisfy the free moment conditions along the free edge of the re-entrant corner.

The effects of adding corner functions to the admissible set of polynomials in the Ritz method on the determination of the frequencies of a plate were investigated through convergence studies for various plates with different shapes. It was shown there that use of corner functions accelerates the convergence of the solutions significantly, thereby permitting one to obtain accurate frequencies from smaller eigenvalue determinants, and reducing numerical ill-conditioning.

The highly accurate results obtained from the present solution were demonstrated through comparison with previously published data for cantilevered triangular, trapezoidal and parallelogram plates. Significant improvement (closer upper bounds) was seen especially for the thick plates with a large skewed angle ($\beta \geq 45^{o}$).

Because of the limitation in the number of pages in this report, only a part of the results from this project were shown. However, we have achieved the goals of the project given in the proposal. We are preparing a paper, which will be submitted to *International Journal of Mechanical Science*. In this paper, a complete set of results for accurate vibration frequencies of skewed cantilevered trapezoidal plates with various skew angles, aspect ratios (*a/b*), chord ratios (*c/b*) and thickness ratios (*h/b*) will be reported and compared to the published results obtained by other researchers to improve the currently available data base.

5. References

[1] Leissa AW. Vibration of plates. NASA SP-160, U.S. Government Printing Office, 1969; Reprinted by The Acoustical Society of America, 1993.

[2] Leissa AW. Recent research in plate vibrations, 1973-1976: Classical theory. The Shock and Vibration Digest 1977; 9(10): 13-24.

[3] Leissa AW. Plate vibration research, 1976-1980: Classical theory. The Shock and Vibration Digest 1981; 13(9): 11-22.

[4] Leissa AW. Recent studies in plate vibrations: 1981-1985. Part I. Classical theory. The Shock and Vibration Digest 1987; 19(2): 11-18.

[5] McGee OG, Leissa AW, Huang CS. Vibrations of cantilevered skewed plates with corner stress singularities. International Journal of Numerical Methods in Engineering 1992; 35(2): 409-424.

[6] McGee OG, Leissa AW, Huang CS. Vibrations of cantilevered skewed trapezoidal and triangular plates with corner stress singularities. International Journal of Mechanical Science 1992; 34(1): 63-84.

[7] McGee OG, Butalia TS. Natural vibrations of shear deformable cantilevered skew trapezoidal and triangular thick plates, Computers & Structures1992; 45(5/6):1033-1059.

[8] Karunasena W, Kitipornchai S, AL-Bermani FGA. Free vibration of cantilevered arbitrary triangular Mindlin plates. International Journal of Mechanical Sciences 1996; 38(4): 431-442.

[9] Kanaka Raju K, Hinton E. Natural frequencies and modes of rhombic Mindlin plates. Earthquake Engineering and Structural Dynamics 1980; 8: 55-62.

[10] Liew KM, Xiang Y, Kitipornchai S, Wang CM. Vibration of thick skew plates based on Mindlin shear deformation plate theory. Journal of Sound and Vibration 1993; 168(1): 39-69.

[11] McGee OG, Leissa AW. Three-dimensional free vibrations of thick skewed cantilevered plates. Journal of Sound and Vibration 1991; 144: 305-322.

[12] McGee OG, Butalia TS. Natural vibrations of shear deformable cantilevered skew thick plates. Journal of Sound and Vibration 1994; 176(3): 351-376.

[13] Huang CS. Stress singularities at angular corners in first-order shear deformation plate theory. International Journal of Mechanical Sciences 2003; 45: 1-20.

[14] Huang CS. On the singularity induced by boundary conditions in a third-order thick plate theory. Journal of Applied Mechanics, ASME 2002; 69: 800-810.

Table 1 Convergence of frequency parameter Ω for a thin triangular plate
(a/b=1, $\beta = 75^o$, h/b=0.001)

Mode No.	K and N in eq. (10) (No. of corner functions)	(I, J) in eq.(9)						McGee et al. [6]
		(4,4)	(5,5)	(6,6)	(7,7)	(8,8)	(9,9)	
1	0	8.251	7.835	7.677	7.272	6.721	6.651	6.437
	5	7.792	6.689	6.484	6.436	6.435	6.435	
	10	6.882	6.457	6.435	6.434	6.434	6.433	
	15	6.450	6.435	6.434	6.433	6.433	6.432	
2	0	32.56	31.13	30.37	29.47	28.84	27.92	27.75
	5	30.87	29.44	28.27	27.74	27.74	27.73	
	10	29.95	28.01	27.74	27.73	27.73	27.72	
	15	27.85	27.73	27.73	27.73	27.72	27.72	
3	0	76.20	72.32	71.22	69.86	68.28	67.69	66.85
	5	73.10	68.11	66.90	66.81	66.81	66.80	
	10	68.01	66.87	66.81	66.80	66.79	66.79	
	15	66.86	66.81	66.80	66.79	66.79	66.78	
4	0	139.2	131.6	128.5	123.2	120.4	118.3	117.9
	5	133.0	118.5	117.9	117.9	117.8	117.8	
	10	120.2	117.9	117.8	117.8	117.8	117.8	
	15	117.9	117.8	117.8	117.7	117.7	117.7	
5	0	209.8	179.3	165.5	154.1	151.0	146.4	144.3
	5	185.7	148.5	144.7	144.3	144.3	144.2	
	10	154.4	144.5	144.3	144.2	144.2	144.1	
	15	144.4	144.3	144.3	144.2	144.1	144.1	

Table 2 Convergence of frequency parameter Ω for a thick triangular plate

(a/b=1, $\beta = 60^{o}$, h/b=0.2)

Mode No.	K and N in eqs. (10a)-(10c) (No. of corner functions)	(I, J) in eqs.(9a)-(9c)						Karunasena et al. [8]
		(4,4)	(5,5)	(6,6)	(7,7)	(8,8)	(9,9)	
1	0	6.314	5.747	5.624	5.500	5.483	5.424	5.517
	5	5.622	5.534	5.458	5.410	5.410	5.409	
	10	5.509	5.449	5.409	5.409	5.409	5.408	
	15	5.432	5.409	5.409	5.408	5.408	5.408	
2	0	25.16	21.26	20.49	20.14	19.95	19.94	20.32
	5	20.98	20.42	20.00	19.93	19.93	19.92	
	10	20.29	20.20	19.93	19.93	19.92	19.92	
	15	19.99	19.93	19.92	19.92	19.92	19.91	
3	0	40.79	29.38	25.27	24.49	23.33	23.22	23.65
	5	27.39	24.64	23.98	23.20	23.19	23.19	
	10	24.56	23.41	23.19	23.19	23.19	23.19	
	15	23.28	23.19	23.19	23.19	23.18	23.18	
4	0	87.98	66.92	46.68	40.92	34.89	34.80	35.43
	5	69.74	44.60	38.92	34.75	34.75	34.75	
	10	41.03	38.01	34.75	34.75	34.75	34.74	
	15	35.66	34.75	34.74	34.74	34.74	34.73	
5	0	101.7	76.13	47.29	43.74	42.16	41.74	41.90
	5	80.46	46.95	42.45	41.27	41.27	41.27	
	10	47.37	41.75	41.27	41.27	41.26	41.26	
	15	41.66	41.27	41.26	41.26	41.25	41.25	

Table 3 Comparison of frequency parameters Ω for trapezoidal thick plates (h/b=0.2)

a/b	c/b	β (degrees)	Mode Number 1	2	3	4
0.5	0.25	15	3.508 <3.521>	7.602 <7.674>	12.71 <12.86>	14.43 </>
		30	3.551 <3.565>	7.882 <7.947>	12.97 <13.06>	14.52 <14.65>
		45	3.724 <3.747>	8.823 <8.897>	13.25 <13.27>	15.77 </>
		60	4.017 <4.026>	10.03 <10.05>	13.26 <13.29>	18.40 </>
		75	4.448 <4.455>	7.244 <7.633>	12.33 <14.63>	15.05 </>
	0.5	15	3.314 <3.330>	6.087 <6.147>	11.36 <11.40>	12.00 <12.00>
		30	3.461 <3.472>	6.396 <6.451>	11.82 <11.90>	12.34 <12.47>
		45	3.736 <3.759>	7.407 <7.410>	12.41 <12.53>	13.49 <13.52>
		60	4.126 <4.135>	9.701 <9.764>	12.92 <12.88>	15.71 </>
		75	4.674 <4.653>	7.780 <8.139>	12.85 <13.93>	13.54 </>
1.0	0.25	15	4.168 <4.170>	14.26 <14.32>	19.42 <19.52>	30.91 </>
		30	4.152 <4.153>	14.43 <14.49>	20.11 <20.22>	30.43 </>
		45	4.275 <4.278>	15.73 <15.80>	21.17 <21.27>	32.31 </>
		60	4.475 <4.494>	17.99 <18.08>	22.16 <22.18>	36.72 </>
		75	4.803 <4.817>	17.90 <18.19>	20.43 <20.54>	34.60 </>
	0.5	15	3.772 <3.774>	11.40 <11.44>	18.42 <18.53>	27.55 </>
		30	3.858 <3.864>	11.76 <11.81>	19.39 <19.52>	27.16 </>
		45	3.858 <3.864>	11.76 <11.81>	19.39 <19.52>	27.16 </>
		60	4.243 <4.444>	16.06 <16.25>	22.31 <22.50>	34.60 </>
		75	4.718 <4.887>	19.21 <19.61>	21.59 <21.68>	35.56 </>

Note: < > denotes values from McGee and Butalia [7];
/ denotes no data available.
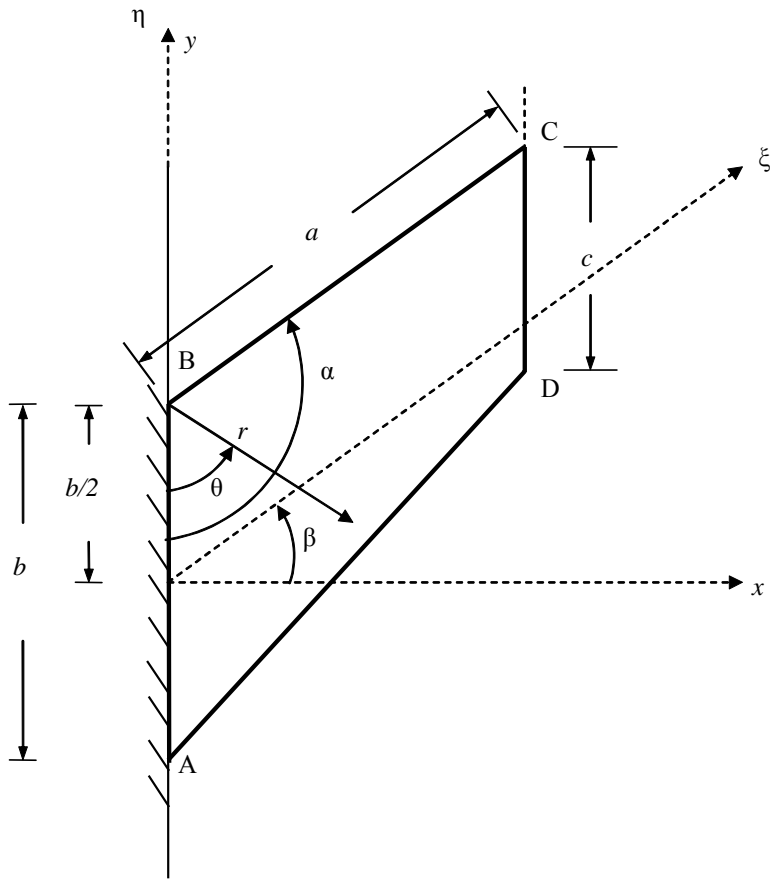
Fig. 1 Geometry and coordinate systems of skewed cantilevered trapezoidal plate.
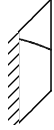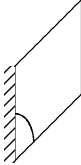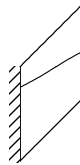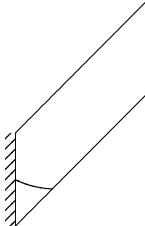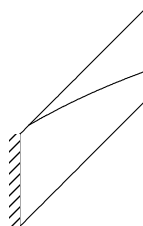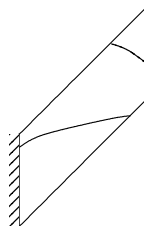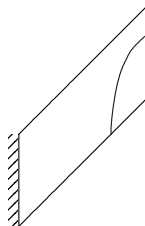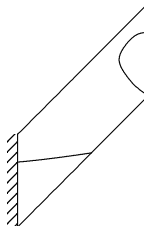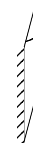
β	a/b	Mode				
		1	2	3	4	5
45°	0.5	(4.236)	(7.359)	(11.38)	(18.29)	(21.22)
	1.0	(4.384)	(10.52)	(24.72)	(28.24)	(44.97)
	2.0	(4.009)	(17.14)	(28.49)	(47.35)	(78.85)
75°	0.5	(5.693)	(21.19)	(25.12)	(36.22)	(39.67)
	1.0	(5.295)	(22.95)	(44.78)	(64.09)	(85.48)
	2.0	(5.018)	(25.51)	(59.77)	(64.91)	(107.4)

Fig. 2   Nodal pattern for parallelogram plates (*h/b*=0.1)

13